Generation of Bessel-beam arrays for parallel fabrication in two-photon polymerization

He Cheng, Chun Xia, Stephen M. Kuebler, Pooria Golvari, Mingman Sun, Meng Zhang, and Xiaoming Yu

COLLECTIONS

View Online   Export Citation   CrossMark

ARTICLES YOU MAY BE INTERESTED IN

Generation of Bessel-beam arrays for parallel fabrication in two-photon polymerization

View Online   Export Citation   CrossMark

He Cheng,[1] Chun Xia,[1] Stephen M. Kuebler,[1,2] Pooria Golvari,[2] Mingman Sun,[3] Meng Zhang,[3] and Xiaoming Yu[1,a]

AFFILIATIONS

[1]CREOL, The College of Optics and Photonics, University of Central Florida, Orlando, Florida 32816
[2]Department of Chemistry, University of Central Florida, Orlando, Florida 32816
[3]Department of Industrial and Manufacturing Systems Engineering, Kansas State University, Manhattan, Kansas 66506

Note: Paper published as part of the special topic on Proceedings of the International Congress of Applications of Lasers & Electro-Optics 2020.
[a]Electronic mail: yux@creol.ucf.edu

ABSTRACT

Microfabrication based on two-photon polymerization (TPP) is typically achieved by scanning a focal spot point-by-point. This is a type of serial processing that significantly limits fabrication speed. Bessel beams known for their nondiffracting property are suitable for the fabrication of high-aspect-ratio microstructures without scanning the beams. The zero-order Bessel beam generated by an axicon or a spatial light modulator (SLM) has been used to fabricate such structures as polymer fibers with an aspect ratio exceeding 500:1. However, the fabrication speed is still limited by the serial exposure of a single Bessel beam. In this paper, the authors explore a method for parallel fabrication of high-aspect-ratio microstructures using an array of high-order Bessel beams. An optics system is built in which high-order and superposed high-order Bessel beams generated by an SLM are demagnified and relayed to the photopolymer. These beams retain the same nondiffracting property as the zero-order beam while expanding the exposure light field to arrays of beams. Beam profiles are characterized and compared with theoretical predictions. The power efficiency of the system is measured and analyzed. The influence of off-axis illumination on the SLM is studied. Combined with suitable photopolymer and exposure parameters, this method could be useful for high-speed, volumetric fabrication in TPP.

Key words: two-photon polymerization, high order Bessel beam, volumetric fabrication

I. INTRODUCTION

Two-photon polymerization (TPP) using femtosecond lasers provides a way for fabricating three-dimensional (3D) structures with high precision.[1] A commonly used method in TPP is point-by-point scanning.[2] However, this method is time-consuming. Various methods have been proposed to increase fabrication speed and throughput, such as multi-focus scanning[3] and projection.[4] Another approach is to use beam shaping to achieve volumetric printing, i.e., 3D structures are fabricated without scanning. Due to its nondiffracting properties, the zero-order Bessel beam produced by an axicon has been used to fabricate high-aspect-ratio structures with single exposure.[5–9] The fabrication speed can be further increased using multiple nondiffracting beams in parallel.

Such beams have been achieved by holograms[10–12] or microaxicon arrays.[13–15] However, the spacing between each beamlet cannot be very small due to interference for the former method and geometric constraint for the latter. On the other hand, nondiffracting beam arrays can be generated by superposing high-order Bessel modes.[16–18] These arrays have tightly packed foci whose patterns can be flexibly designed using a proper choice of fundamental Bessel modes, so they could be a good candidate for fabricating high-aspect-ratio array structures in parallel.

In this paper, we develop an analytical expression for the superposed high-order Bessel beams generated by displaying holograms on a spatial light modulator (SLM) and relaying them by a 4f system. We confirm the validity of the model by comparing with simulation results and experimental results.

II. THEORY

It has been found that an axiconlike phase mask combined with azimuthal modulation produces a nondiffracting beam,[19]

$$t(r', \phi') = A(\phi')e^{-ik_r r'}, \tag{1}$$

where (r', ϕ') are polar coordinates on the mask plane, k_r is a constant (corresponding to the radial component of the wave number), and $A(\phi')$ is a complex function. When $A(\phi') = 1$, the phase term $e^{-ik_r r'}$ alone produces a conical wave, which is an approximation of the zero-order Bessel beam.[20–22] In this case, the function $t(r', \phi')$ represents the complex transmittance function of a thin axicon.

High-order Bessel beams of the order m can be approximately produced by choosing $A(\phi') = e^{im\phi'}$, where m is an integer.[23] This transmittance function can be displayed on a SLM with a circular aperture of the radius R. After illuminating the SLM with a Gaussian beam and ignoring pixelization of the SLM panel, the reflected complex field can be written as

$$E_m(r', \phi', z' = 0) = e^{-(r'^2/w_0^2)}e^{-ik_r r'}e^{im\phi'}\text{circ}\left(\frac{r}{R}\right), \tag{2}$$

where w_0 is $1/e^2$ radius of Gaussian beam, z' is the coordinate along the optical axis, circ(r) is the circle function which equals 1 when $0 < r < 1$ and equals 0 otherwise. Using the Fresnel diffraction integral in cylindrical coordinates, we can write the complex field after the SLM as

$$E(r, \phi, z) = \frac{1}{i\lambda z}e^{ikz}e^{i(kr^2/2z)}\int_0^R dr'r'e^{i(kr'^2/2z)}e^{-(r'^2/w_0^2)}e^{-ik_r r'}$$
$$\times \int_0^{2\pi} d\phi' \, e^{im\phi'}e^{-i(krr'/z)\cos(\phi-\phi')}, \tag{3}$$

where $k = 2\pi/\lambda$ is the wave number and (r, ϕ, z) are the cylindrical coordinates. Using the integral representation of the Bessel function,[24] the second integral in Eq. (3) can be calculated as

$$\int_0^{2\pi} d\phi' \, e^{im\phi'}e^{-i(krr'/z)\cos(\phi-\phi')} = 2\pi(-i)^m e^{im\phi}J_m\left(\frac{krr'}{z}\right), \tag{4}$$

where $J_m(x)$ represents the mth-order Bessel function of the first type. Inserting Eq. (4) into Eq. (3) gives

$$E_m(r, \phi, z) = \frac{1}{i\lambda z}e^{ikz}e^{i(kr^2/2z)}2\pi(-i)^m e^{im\phi} \times \int_0^R dr'f(r')e^{ik\mu(r')}, \tag{5}$$

where functions $f(r')$ and $\mu(r')$ are

$$f(r') = r'e^{-(r'^2/w_0^2)}J_m\left(\frac{krr'}{z}\right) \tag{6}$$

and

$$\mu(r') = \frac{r'^2}{2z} - \frac{k_r}{k}r'. \tag{7}$$

Because the phase term in the integrand in Eq. (5) varies rapidly, the integral can be evaluated asymptotically using the stationary phase method.[25,26] There is only one critical point $r'_c = k_r z/k$ within the interval $0 < z < kR/k_r$ at which the first derivative of $\mu(r'_c)$ equals zero. The leading contribution of the integral in Eq. (5) can be expressed as

$$\int_0^R dr'f(r')e^{ik\mu(r')} \approx f(r'_c)e^{ik\mu(r'_c)}\sqrt{\frac{2\pi i}{k\mu''(r'_c)}}, \tag{8}$$

where $\mu''(r')$ represents the second derivative of $\mu(r')$. The approximation is valid only when the variation of $f(r')$ in the stationary phase regions is small, requiring $r^2 \ll z\lambda/4$.[23] Substituting the result above into Eq. (5) yields the complex field after the SLM as

$$E_m(r, \phi, z) = (2\pi)^{3/2}(-1)^m(i)^{m-(1/2)}\lambda^{-1}k_r k^{-(3/2)}$$
$$\times z^{1/2}e^{-(k_r^2/k^2 w_0^2)z^2}e^{i(kz + (kr^2/2z) - (k_r^2/2k)z)}e^{im\phi}J_m(k_r r). \tag{9}$$

E_m in Eq. (9) approximates a Bessel beam of the mth-order with finite depth of field.

Now, we can superpose two complex transmittance functions $t(r', \phi')$ in Eq. (1) with the order of l and m and display it on the SLM as

$$t_{l+m}(r', \phi') = (e^{il\phi'} + e^{im\phi'})e^{-ik_r r'}. \tag{10}$$

After propagation, the resulting beam is a linear combination of the mth- and lth-order Bessel beams, and the intensity distribution $I(r, f, z)_{l+m}$ is

$$I(r, \phi, z)_{l+m} \propto |E_l(r, \phi, z) + E_m(r, \phi, z)|^2$$
$$= ze^{-(2k_r^2/k^2 w_0^2)z^2}\{|C_l|^2 J_l^2(k_r r)|C_m|^2 J_m^2(k_r r)$$
$$+ 2|C_l||C_m|J_l(k_r r)J_m(k_r r)\cos[(l-m)\phi + \theta_{lm}]\}. \tag{11}$$

Here, C_l and C_m represent the constant terms in front of $J_l(k_r r)$ and $J_m(k_r r)$ in Eq. (9), and $C_l C_m = |C_l||C_m|e^{i\theta_{lm}}$. Note that the variables z and r are separated in Eq. (11), meaning that the transverse intensity profile remains the same as the beam propagates along the z axis, although its peak intensity does vary. The first term on the right-hand side of Eq. (11) containing z describes the intensity distribution along the propagation axis. Its form is similar to the Rayleigh distribution, which physically means the beam has a limited depth of field compared to a theoretical nondiffracting beam. This behavior is also observed for a Gaussian–Bessel beam generated by illuminating an axicon with a Gaussian beam.[27,28] It can be seen from Eq. (11) that the transverse profile has $|l - m|$-fold symmetry.

The aforementioned procedure can be used to generate other transverse profiles of this group of nondiffracting beams from a superposition of multiple orders,

$$I(r, \phi, z) \propto \left|\sum_n c_n E_n(r, \phi, z)\right|^2, \tag{12}$$

where n is an integer. In this work, we limit our discussion to two- and three-component superpositions. In order to apply such beams
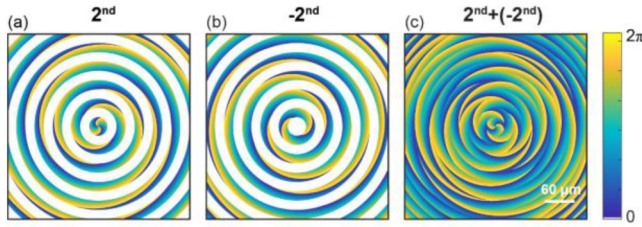
FIG. 1. Constructing the phase map for superposition of two Bessel beams with order $l = 2$ and $m = -2$ using Eq. (14). (a) Phase map of order $l = 2$ (14). (b) Phase map of order $m = -2$. (c) Phase map of superposed orders. Note that (a) and (b) have phase information encoded in an alternating fashion along the radial direction.

in microfabrication like two-photon polymerization (TPP),[5] the beams need to be demagnified ("focused"). Typically, a 4f system is used to relay the beam into the photopolymer by putting the SLM at the "object plane" (back focal plane of the first lens of the 4f system). Assuming that the magnification of the 4f system is $1/M$, the complex field at the image plane (front focal plane of second lens of the 4f system) will be an inverted, $1/M$-scaled image of the SLM. Then, the field after the image plane can be derived as described above, giving

$$
\begin{aligned}
I_{l+m}'^{(r,\phi,z)} &\propto |E'_l(r,\,\phi,\,z) + E'_m(r,\,\phi,\,z)|^2 \\
&= z\,e^{-(2k_r'^2/k^2 w_0'^2)z^2}\{|C_l|^2 J_l^2(k'_r r) + |C_m|^2 J_m^2(k'_r r) \\
&\quad + 2|C_l||C_m| J_l(k'_r r) J_m(k'_r r)\cos((l-m)(\phi+\pi) + \theta_{lm})\}.
\end{aligned}
\tag{13}
$$

Comparing Eq. (13) with Eq. (11), we find the image-scaling parameters appear in $k'_r = Mk_r$ and $w'_0 = w_0/M$. Thus, the depth of field is decreased by M^2 and the transverse profile is scaled by $1/M$, which is consistent with basic object-image relationships.

III. SIMULATION

We are considering phase-only SLMs that are commonly used in TPP. The transmittance function described in Eq. (10) cannot be directly displayed on such SLMs due to the lack of amplitude modulation. The amplitude information of a complex field can be coded into the phase map[29] at the expense of sacrificing power efficiency. Another method is to imprint the two phase terms in Eq. (10) alternatively along the radial direction,[16,17] which is used here. The transmittance function for superposing two Bessel beams is

$$
\begin{aligned}
T_{l+m}(r',\,\phi') &= \exp(-ik_\perp r') \\
&\times \left[\frac{(-1)^{\text{floor}(\frac{r'}{\Delta})} + 1}{2} e^{il\phi'} - \frac{(-1)^{\text{floor}(\frac{r'}{\Delta})} - 1}{2} e^{im\phi'} \right].
\end{aligned}
\tag{14}
$$

These phase maps consist of concentric rings with azimuthal modulation, where Δ is the width of each ring, and floor(x) is the floor function that outputs the largest integer smaller than or equal to a real number x. Figure 1 shows an example of a phase map for the superposition of 2nd- and $-$2nd-order Bessel beams.

The principles for superposing three or more Bessel beams are the same. However, we observe a reduction in quality of the generated beams with an increasing number of superposed beams using this method. In simulation, we fix Δ to $18.4\,\mu$m, corresponding to the size of two pixels on the SLM. We find that good results can be achieved when Δ is in range of one pixel ($9.2\,\mu$m) to several pixels.

In our simulation, the SLM has a circular aperture of 9 mm in radius and a pixel pitch of $9.2\,\mu$m. The SLM is placed at the object plane of a 4f system, which consists of two lenses with a focal length of 700 and 25 mm and the same aperture radius (8 mm), resulting in a magnification of $1/M$=1/28. A Gaussian beam with a $1/e^2$ radius of 10 mm is incident perpendicularly on the SLM. A beam splitter in front of the SLM would be needed to achieve this normal incidence if a reflective SLM is used. Alternatively, the configuration of oblique incidence (and thus oblique reflection) on the SLM without a beam splitter is preferred for increased energy
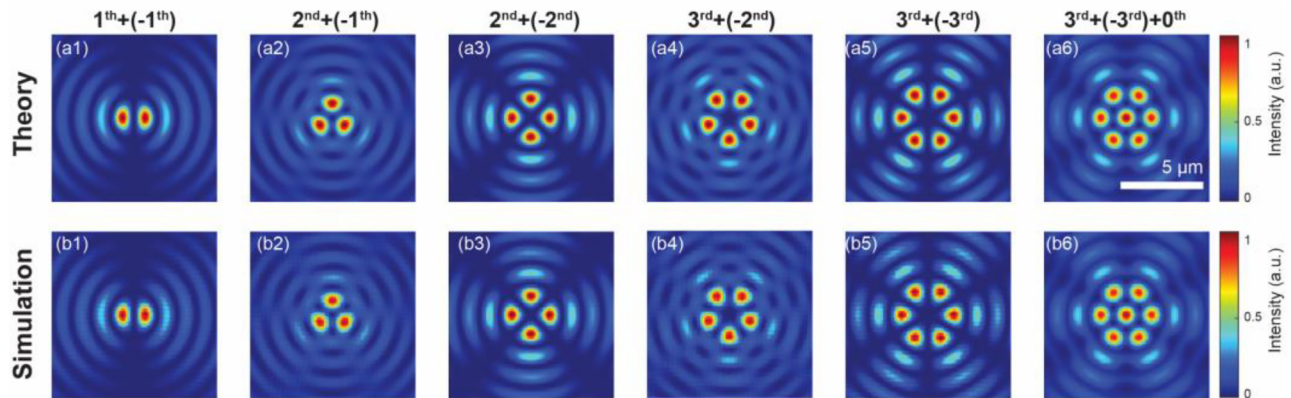

FIG. 2. Transverse profiles of superposed Bessel beams from the theory and simulation. The profiles are obtained at $z = 0.6$ mm.
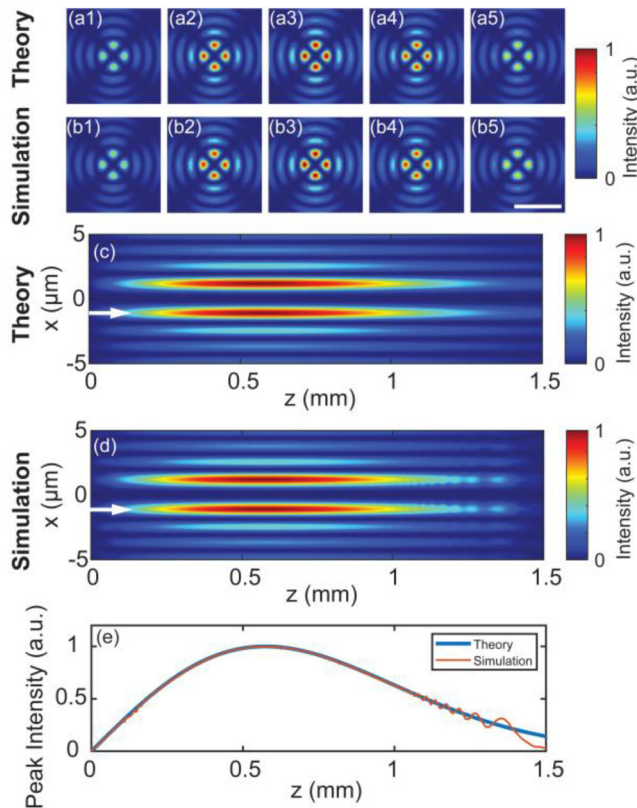
FIG. 3. Propagation of the (2nd) + (−2nd) order Bessel beam. (a1)–(a5) Theoretical calculation and (b1)–(b5) simulation of the transverse intensity profile at $z = 0.2$, 0.4, 0.6, 0.8, and 1 mm, respectively. (c) and (d) Calculated and simulated intensity distribution along the propagation direction at the xz plane ($y = 0$). (e) Peak intensity as a function of z. White arrows indicate the locations of peak intensity measurements. Scale bar: 5 μm.

efficiency. However, in the second setup, the beam quality could be reduced due to the aberration caused by the tilted SLM.[30,31] The complex field at and after the image plane of the 4f system is obtained by numerically evaluating the Fresnel diffraction integrals using the angular spectrum method.[32] The simulation results show a diffraction efficiency of 50%. The extra energy loss is because the encoding method shown in Fig. 1 introduces higher diffraction orders. Note that in the simulation, the fill factor of the SLM is assumed to be 100%, so the energy loss due to pixelization of the SLM is not considered.

Figure 2 shows the transverse profiles of superposed Bessel beams with various orders from theoretical calculation and simulation results at $z = 0.6$ mm. Parameter z is measured along the optical axis and $z = 0$ at the image plane of the 4f system. The theoretical calculation is in good agreement with the simulation results. The transverse profiles have $|l - m|$-fold symmetry, which agrees with prediction from theory.

The nondiffracting property of a superposed Bessel beam is demonstrated in Fig. 3, which compares the theoretical calculation with simulation results and the good agreement between them. We observe that the transverse beam profiles remain unchanged apart from the peak intensities, over a distance longer than 1 mm [Figs. 3(a) and 3(b)]. The axial intensity measurement along the propagation direction [Fig. 3(e)] agrees with the term $z \exp[-2k_r'^2 z^2/(k^2 w_0'^2)]$ in Eq. (13) that describes the distribution along the propagation direction. The oscillations observed at the end of the beam in the simulation results are due to the diffraction by the aperture edge of SLM, which are not included in the theoretical calculation.

The nondiffracting property of superposed Bessel beams makes them a candidate for fabricating high-aspect-ratio structures in parallel. Both the theoretical calculation and simulation results indicate that the axial intensity distributions are nearly identical for superposed Bessel beams with different orders (transverse profiles shown in Fig. 2). This can be seen from Eq. (13) in which the leading term that describes the axial intensity is not related to the orders of
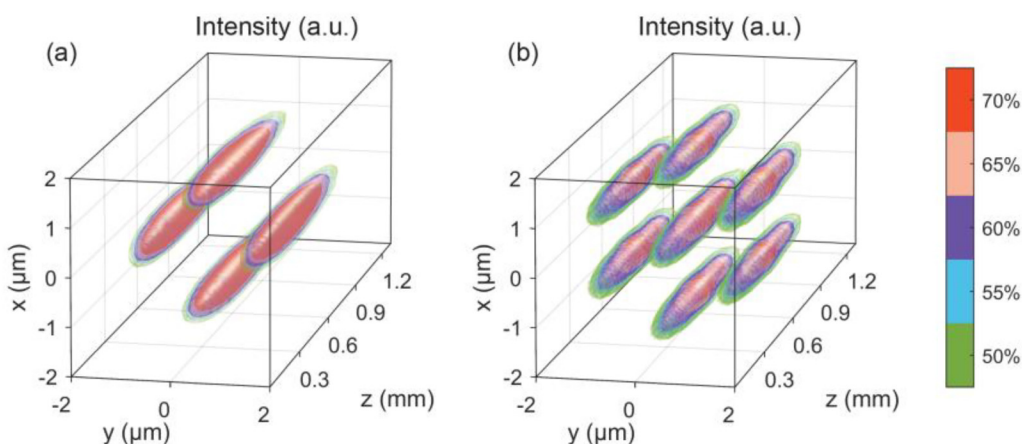

FIG. 4. Iso-intensity representation of simulated superposed Bessel beams. (a) Superposed 2nd- and −2nd-order Bessel beam. (b) Superposed 3rd-, −3rd-, and 0th-order Bessel beam. The intensity is normalized to the respective peak intensities for both cases.

Bessel beams nor the transverse profile. This suggests the flexibility of shaping the transverse profile by combining different numbers and orders of Bessel beams, without affecting the axial profile.

One possible application is fabricating high-aspect-ratio arrays by single exposure. The superposed Bessel beams shown in Fig. 2 with well-defined and tightly packed "petals" (the distance between each petal is less than $1\,\mu m$) and good contrast between the petals and low-intensity region may be particularly suitable for this task. Figure 4 demonstrates the three-dimensional shape for two examples of a superposed Bessel beam. These iso-intensity plots are drawn using a cutoff that is 50% of the peak intensity, meaning that the "sidelobes" outside the petals have a maximum intensity <50% of the peak intensity in each petal. In TPP where nonlinear processes are involved, the threshold condition is proportional to the square of intensity. In this case, the contrast of the transverse profiles will be higher, making it easier to fabricate well-defined structures.

Due to the symmetry of the transverse profiles, these superposed beams could be helpful in fabricating two- or three-dimensional structures with repeating patterns.[33,34] The beams shown in Figs. 2(a2) and 2(a6) can be used as a basis in fabricating structures with a repeating triangular pattern. The beam shown in Fig. 2(a3) can be used for a repeating square pattern and the beam shown in Fig. 2(a5) can be used for a repeating hexagonal pattern (such as a honeycomb). There are other patterns that can be achieved by either offsetting the location of each basis or combining multiple bases. The fabrication throughput could be significantly increased when utilizing this method, especially for three-dimensional fabrication.

IV. EXPERIMENT

The experimental setup used for characterization of a superposed Bessel beam is schematically shown in Fig. 5. The laser source is a commercial femtosecond laser system. It outputs 170 fs pulses at a repetition rate of 1 kHz. The center wavelength of the laser pulse is 1030 nm. The laser beam has a nearly Gaussian shape with $1/e^2$ radius of 2.5 mm. The laser beam is frequency-doubled by second harmonic generation and expanded to a collimated beam
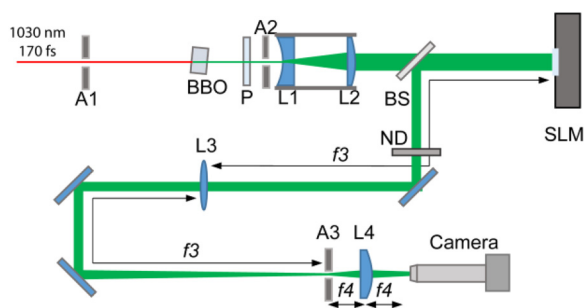

FIG. 5. Schematic of the experimental setup. A1, A2, and A3, iris diaphragms; BBO, beta barium borate; P, polarizer; L1, $f = -25$ mm lens; L2, $f = 100$ mm lens; BS, beam splitter; SLM, spatial light modulator; L3, $f3 = 750$ mm lens; L4, $f4 = 26$ mm lens; ND, neutral density filter.
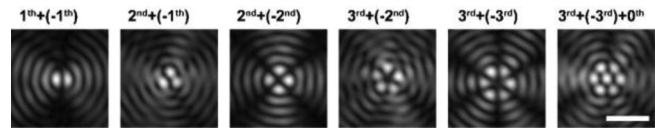

FIG. 6. Transverse intensity distribution of superposed Bessel beams. Scale bar: $5\,\mu m$.

with a diameter of 20 mm. Spatial modulation of the transverse beam phase are produced through reflecting the beam off the computer controlled spatial light modulator (Meadowlark Optics). Then, the modulated beam is redirected to the 4f system by the beam splitter. Not accounting for the loss introduced by lenses, mirrors, and the beam splitter, the efficiency of transformation from the input beam into the superposed Bessel beam is about 25%.

Superposed Bessel beams are further reduced in size, by $M = 28.8$ times, using a 4f system composed of a 750 and a 26 mm lens. The resulting superposed Bessel beam is located near the back focal plane of L4. The beam profile is then captured by a camera mounted on a translation stage. Examples of the transverse intensity profiles of superposed Bessel beams with selected orders are shown in Fig. 6. The superposed Bessel beam has a nondiffraction range of about 1 mm. Distortion in the transverse beam profile can be observed, which is mainly due to aberration from L4 with short focal distance. The transverse intensity distributions are close to simulation and theoretical results. Further improvement in the beam profile quality can be achieved by replacing L4 with a high-quality lens with minimal aberration.

V. CONCLUSION

We have demonstrated a theoretical model to describe the superposed high-order Bessel beam arrays produced by an SLM and relayed by a 4f system. The theoretical calculation shows a good agreement in the beam profile with numerical simulation. A preliminary experimental result shows that the transverse intensity profiles are very close to theoretical prediction and simulation results. With the 4f system, the superposed high-order Bessel beams show tightly packed foci while remain the nondiffracting property like the zero-order Bessel beam. The symmetry of their transverse profiles makes them particularly useful for the parallel fabrication of high-aspect-ratio structures with repeating patterns.

ACKNOWLEDGMENT

REFERENCES

[1]S. Kawata, H. B. Sun, T. Tanaka, and K. Takada, "Finer features for functional microdevices," Nature **412**, 697–698 (2001).
[2]M. Farsari and B. N. Chichkov, "Materials processing: Two-photon fabrication," Nat. Photonics **3**, 450–452 (2009).
[3]G. Vizsnyiczai, L. Kelemen, and P. Ormos, "Holographic multi-focus 3D two-photon polymerization with real-time calculated holograms," Opt. Express **22**, 24217–24223 (2014).

[4]L. Yang, J. Li, Y. Hu, C. Zhang, Z. Lao, W. Huang, and J. Chu, "Projection two-photon polymerization using a spatial light modulator," Opt. Commun. **331**, 82–86 (2014).

[5]H. Cheng, C. Xia, M. Zhang, S. M. Kuebler, and X. Yu, "Fabrication of high-aspect-ratio structures using Bessel-beam-activated photopolymerization," Appl. Opt. **58**, D91–D97 (2019).

[6]X. Yu, M. Zhang, and S. Lei, "Multiphoton polymerization using femtosecond Bessel beam for layerless three-dimensional printing," J. Micro Nano Manuf. **6**, 010901 (2018).

[7]J. Jezek, T. Cizmár, V. Nedela, and P. Zemánek, "Formation of long and thin polymer fiber using nondiffracting beam," Opt. Express **14**, 8506–8515 (2006).

[8]F. Courvoisier, R. Stoian, and A. Couairon, "Ultrafast laser micro- and nano-processing with nondiffracting and curved beams," Opt. Laser Technol. **80**, 125–137 (2016).

[9]M. Duocastella and C. B. Arnold, "Bessel and annular beams for materials processing," Laser Photonics Rev. **6**, 607–621 (2012).

[10]P. García-Martínez, M. M. Sánchez-López, J. A. Davis, D. M. Cottrell, D. Sand, and I. Moreno, "Generation of Bessel beam arrays through Dammann gratings," Appl. Opt. **51**, 1375–1381 (2012).

[11]R. Bowman, N. Muller, X. Zambrana-Puyalto, O. Jedrkiewicz, P. Di Trapani, and M. J. Padgett, "Efficient generation of Bessel beam arrays by means of an SLM," Eur. Phys. J. Spec. Top. **199**, 159–166 (2011).

[12]S. H. Tao, X.-C. Yuan, and B. S. Ahluwalia, "The generation of an array of nondiffracting beams by a single composite computer generated hologram," J. Opt. A Pure Appl. Opt. **7**, 40–46 (2005).

[13]E. Stankevicius, M. Garliauskas, and G. Raciukaitis, "Bessel-like beam array generation using round-tip micro-structures and their use in the material treatment," J. Laser Micro Nanoeng. **11**, 352–356 (2016).

[14]E. Stankevičius, M. Garliauskas, M. Gedvilas, and G. Račiukaitis, "Bessel-like beam array formation by periodical arrangement of the polymeric round-tip microstructures," Opt. Express **23**, 28557–28566 (2015).

[15]R. Grunwald, U. Griebner, F. Tschirschwitz, E. T. J. Nibbering, and T. Elsaesser, "Generation of femtosecond Bessel beams with microaxicon arrays," Opt. Lett. **25**, 981 (2000).

[16]X. Yu, C. A. Trallero-Herrero, and S. Lei, "Materials processing with superposed Bessel beams," Appl. Surf. Sci. **360**, 833–839 (2016).

[17]L. Yang, D. Qian, C. Xin, Z. Hu, S. Ji, D. Wu, Y. Hu, J. Li, W. Huang, and J. Chu, "Two-photon polymerization of microstructures by a non-diffraction multifoci pattern generated from a superposed Bessel beam," Opt. Lett. **42**, 743–746 (2017).

[18]R. Vasilyeu, A. Dudley, N. Khilo, and A. Forbes, "Generating superpositions of higher–order Bessel beams," Opt. Express **17**, 23389–23395 (2009).

[19]A. Vasara, J. Turunen, and A. T. Friberg, "Realization of general nondiffracting beams with computer-generated holograms," J. Opt. Soc. Am. A **6**, 1748–1754 (1989).

[20]J. Durnin, "Exact solutions for nondiffracting beams. I. The scalar theory," J. Opt. Soc. Am. A **4**, 651–654 (1987).

[21]J. Durnin, J. J. Miceli, and J. H. Eberly, "Diffraction-free beams," Phys. Rev. Lett. **58**, 1499–1501 (1987).

[22]R. M. Herman and T. A. Wiggins, "Production and uses of diffractionless beams," J. Opt. Soc. Am. A **8**, 932–942 (1991).

[23]C. Paterson and R. Smith, "Higher-order Bessel waves produced by axicon-type computer-generated holograms," Opt. Commun. **124**, 121–130 (1996).

[24]E. W. Weisstein, See https://mathworld.wolfram.com/BesselFunctionofthe FirstKind.html for "Bessel function of the first kind."

[25]L. B. Felsen and N. Marcuvitz, *Radiation and Scattering of Waves* (IEEE, New York, 1994).

[26]A. V. Osipov and S. A. Tretyakov, *Modern Electromagnetic Scattering Theory with Applications* (Wiley, New York, 2017).

[27]V. Jarutis, R. Paškauskas, and A. Stabinis, "Focusing of Laguerre–Gaussian beams by axicon," Opt. Commun. **184**, 105–112 (2000).

[28]J. Zheng, Y. Yang, M. Lei, B. Yao, P. Gao, and T. Ye, "Fluorescence volume imaging with an axicon: Simulation study based on scalar diffraction method," Appl. Opt. **51**, 7236–7245 (2012).

[29]J. A. Davis, D. M. Cottrell, J. Campos, M. J. Yzuel, and I. Moreno, "Encoding amplitude information onto phase-only filters," Appl. Opt. **38**, 5004–5013 (1999).

[30]H. Cheng, C. Xia, S. M. Kuebler, and X. Yu, "Aberration correction for SLM-generated Bessel beams propagating through tilted interfaces," Opt. Commun. **475**, 126213 (2020).

[31]A. Thaning, Z. Jaroszewicz, and A. T. Friberg, "Diffractive axicons in oblique illumination: Analysis and experiments and comparison with elliptical axicons," Appl. Opt. **42**, 9–17 (2003).

[32]J. D. Schmidt, *Numerical Simulation of Optical Wave Propagation with Examples in MATLAB* (SPIE, Bellingham, WA, 2010), pp. 95–102.

[33]X. Ao, L. Liu, L. Wosinski, and S. He, "Polarization beam splitter based on a two-dimensional photonic crystal of pillar type," Appl. Phys. Lett. **89**, 171115 (2006).

[34]J. E. Baker, R. Sriram, and B. L. Miller, "Two-dimensional photonic crystals for sensitive microscale chemical and biochemical sensing," Lab Chip **15**, 971–990 (2015).